

Large barocaloric effects in thermoelectric superionic materials

Jie Min, Arun K. Sagotra, and Claudio Cazorla 

School of Materials Science and Engineering, UNSW Sydney, Sydney, New South Wales 2052, Australia



(Received 14 November 2019; published 29 January 2020)

We predict the existence of large barocaloric effects above room temperature in the thermoelectric fast-ion conductor Cu_2Se by using classical molecular dynamics simulations and first-principles computational methods. A hydrostatic pressure of 1 GPa induces large isothermal entropy changes of $|\Delta S| \sim 15\text{--}45 \text{ J kg}^{-1} \text{ K}^{-1}$ and adiabatic temperature shifts of $|\Delta T| \sim 10 \text{ K}$ in the temperature interval $400 \leq T \leq 700 \text{ K}$. Structural phase transitions are absent in the analyzed thermodynamic range. The causes of such large barocaloric effects are significant P -induced variations on the ionic conductivity of Cu_2Se and the inherently high anharmonicity of the material. Uniaxial stresses of the same magnitude, either compressive or tensile, produce comparatively much smaller caloric effects, namely, $|\Delta S| \sim 1 \text{ J kg}^{-1} \text{ K}^{-1}$ and $|\Delta T| \sim 0.1 \text{ K}$, due to practically null influence on the ionic diffusivity of the material. Our simulation work shows that thermoelectric compounds presenting high ionic disorder, like copper and silver-based chalcogenides, may render large mechanocaloric effects and thus are promising materials for engineering solid-state cooling applications that do not require the application of electric fields.

DOI: [10.1103/PhysRevMaterials.4.015403](https://doi.org/10.1103/PhysRevMaterials.4.015403)

I. INTRODUCTION

Conventional cooling technologies are based on compression cycles of greenhouse gases (e.g., hydrofluorocarbons), which pose serious threats to the environment. One kilogram of a typical refrigerant gas is, in terms of greenhouse impact, equivalent to two tons of carbon dioxide, which equals the total emissions produced by a car running uninterruptedly during six months [1]. Current cooling technologies, in addition, present two other important limitations, namely, the energy efficiency of the refrigeration cycles are relatively low (<60%) [2], and they cannot be scaled down to small sizes (e.g., microchip dimensions).

Solid-state cooling is an emergent refrigeration technology that exploits thermal effects in materials and which could solve most of the problems associated with traditional vapor-compression refrigeration. For instance, solid-state cooling systems do not represent any environmental threat in terms of greenhouse gas emissions and in principle can be reduced in size to fit within portable devices. The absence of moving parts and silent operation represent additional advantages over traditional refrigeration technologies. Two broad families of materials that are employed in solid-state cooling applications are caloric [2] and thermoelectric [3] compounds.

Caloric materials react thermally to external coercive fields like electric and magnetic bias [2,4–6] and mechanical stresses [7–10]. Caloric effects result from field-induced transformations that involve large changes in entropy ($\sim 10\text{--}100 \text{ J kg}^{-1} \text{ K}^{-1}$). One typical example of caloric materials are shape-memory alloys (e.g., near equiatomic Ni-Ti alloys), which exhibit superb elastic properties and a martensite to austenite phase transition with a large latent heat that can be triggered by external fields (e.g., uniaxial tensile stress) [7,9]. Solid-state cooling energy efficiencies of $\sim 75\%$ have

been demonstrated for some caloric materials and further improvements appear to be within reach [2,11].

Meanwhile, thermoelectric materials create an electric potential when subjected to a temperature gradient and *vice versa*, that is, they generate a temperature gradient when subjected to an electric bias. Thermoelectric refrigerators exploit the latter effect, known as the Peltier effect, and thus cooling is achieved via the application of electric fields [3,12]. The efficiency of thermoelectric materials is measured by a dimensionless parameter called “thermoelectric figure of merit,” which typically adopts values of ~ 1 for good specimens [13,14]. Unfortunately, the energy efficiency of current thermoelectric refrigerators are relatively low as compared to that of conventional vapor compression systems [15]. In principle, thermoelectric figures of merit much higher than ~ 1 are necessary for thermoelectric coolers to become commercially viable [15].

Copper selenide, Cu_2Se , is an inorganic compound for which recently huge thermoelectric figures of merit of ~ 2 have been reported experimentally at high temperatures ($\sim 1000 \text{ K}$) [16]. Above room temperature, the copper ions in Cu_2Se become highly mobile and the system enters a “superionic” state [17,18] that is characterized by a very low lattice thermal conductivity ($\sim 1 \text{ W m}^{-1} \text{ K}^{-1}$) [16,19]. The resulting “liquidlike” behavior of the Cu ions appears to be the main cause for the huge thermodynamic figure of merit observed in this material. Likewise, large thermoelectric figures of merit have been reported for analogous superionic Cu- and Ag-based chalcogenides like Cu_2S , Cu_2Te , Ag_2Se , Ag_2S , Ag_2Te , and $\text{Cu}_{2-x}\text{Ag}_x\text{X}$ ($X = \text{S, Se and Te}$) alloys [20–22]. Nevertheless, most of such thermoelectric fast-ion conductors exhibit low thermodynamic stability when subjected to strong electric fields owing to undesired electromigration [23,24]. Consequently, these materials are not suitable for engineering

practical solid-state cooling applications based on the Peltier effect due to limiting degradation issues [24].

In this study, we present theoretical evidence showing that thermoelectric superionic materials typified by Cu_2Se may exhibit large caloric effects when subjected to hydrostatic pressure (that is, barocaloric effects). In particular, an isotropic compression of ~ 1 GPa in the temperature interval $400 \leq T \leq 700$ K induces a significant decrease in the ionic diffusivity of Cu_2Se , which translates into a large decrease in lattice entropy and overall enhancement in the thermodynamic stability of the system. Anharmonicity, which is inherently high in superionic materials [25–27], also plays an important role on the estimated large entropy variations. The adiabatic temperature shifts accompanying the barocaloric effects amount to ~ 10 K, which are reasonably large as compared to those reported for other known barocaloric materials. Caloric effects produced by moderate uniaxial stresses (that is, elastocaloric effects), on the contrary, are quite small (~ 0.1 K) due to practically negligible influence on the ionic diffusivity of Cu_2Se . Our study suggests that thermoelectric materials presenting high ionic disorder could be used for engineering solid-state cooling applications that do not require the application of electric fields, thus avoiding potential thermodynamic instability issues.

II. COMPUTATIONAL METHODS

Molecular dynamics (MD) (N, P, T) simulations were performed with the LAMMPS code [28]. The pressure and temperature in the system were kept fluctuating around a set-point value by using thermostatting and barostatting techniques in which some dynamic variables are coupled to the particle velocities and simulation box dimensions. The interactions between atoms were modeled with the Morse potential reported by Namsani *et al.* in work [29]. This potential reproduces within a few percent the structural and elastic properties of Cu_2Se at high temperatures as reported from experiments and first-principles calculations [29]. The Coulombic interactions between ions, however, were neglected in this study in order to reproduce correctly the superionic behavior of Cu_2Se at high temperatures (Sec. III).

We employed large simulation boxes, typically containing 14 000 atoms, and applied periodic boundary conditions along the three Cartesian directions. Off-stoichiometric Cu_2Se configurations were generated by removing a specific number of cations and anions randomly from the simulation cell (in order to fulfill the condition of charge neutrality). Newton's equations of motion were integrated using the customary Verlet's algorithm with a time-step length of 10^{-3} ps. The typical duration of a MD run was of 1 ns. A particle-particle particle-mesh k -space solver was used to compute long-range interactions beyond a cutoff distance of 12 Å at each time step. MD simulations were performed in the thermodynamic intervals $400 \leq T \leq 800$ K and $0 \leq P \leq 1$ GPa by considering thermodynamic variable increments of $\delta T = 25$ K and $\delta P = 0.1$ GPa.

Ab initio molecular dynamics (AIMD) simulations based on density functional theory (DFT) were performed to analyze the ionic transport properties of Cu_2Se and test the reliability of the employed interaction potential. These simulations were

performed in the canonical ensemble (N, V, T) with the VASP code [30] by following the generalized gradient approximation to the exchange-correlation energy due to Perdew *et al.* [31]. The projector augmented-wave method was used to represent the ionic cores [32], and the electronic states Cu $4s-3d$ and Se $4s-4p$ were considered as valence. Wave functions were represented in a plane-wave basis truncated at 650 eV. The temperature in the AIMD simulations was kept fluctuating around a set-point value by using Nose-Hoover thermostats. Simulation boxes containing 288 atoms were used in all the AIMD simulations and periodic boundary conditions were applied along the three Cartesian directions. Newton's equations of motion were integrated using the customary Verlet's algorithm and a time-step length of 10^{-3} ps. Γ -point sampling for integration within the first Brillouin zone was employed in all the AIMD simulations. The total duration of each AIMD run was of ~ 200 ps.

Ionic diffusion coefficients, D_{Cu} and D_{Se} , were calculated with the formula [26]:

$$D_i = \lim_{t \rightarrow \infty} \frac{\langle |R_i(t + t_0) - R_i(t_0)|^2 \rangle}{6t}, \quad (1)$$

where $R_i(t)$ is the position of the migrating ion labeled as i at time t , t_0 an arbitrary time origin, and $\langle \dots \rangle$ denotes average over time and particles. The mean squared displacement of each ionic species is defined as $\langle \Delta R_i^2(t) \rangle \equiv \langle |R_i(t + t_0) - R_i(t_0)|^2 \rangle$.

The isothermal entropy changes associated with barocaloric effects were estimated indirectly by using the corresponding Maxwell relation like [2]:

$$\Delta S(P, T) = \int_0^P \left(\frac{\partial S}{\partial P'} \right)_T dP' = - \int_0^P \left(\frac{\partial V}{\partial T} \right)_{P'} dP', \quad (2)$$

where P represents the maximum applied hydrostatic pressure and V the volume of the system. Likewise, the isothermal entropy changes associated with elastocaloric effects were calculated as [2]:

$$\Delta S(\sigma, T) = \int_0^\sigma \left(\frac{\partial S}{\partial \sigma'} \right)_T d\sigma' = V_0 \int_0^\sigma \left(\frac{\partial \epsilon}{\partial T} \right)_{\sigma'} d\sigma', \quad (3)$$

where σ represents the maximum applied uniaxial stress along an arbitrary Cartesian direction (denoted here as z), ϵ the strain deformation that the system undergoes along the same direction (i.e., $\epsilon(\sigma, T) \equiv \frac{L_z(\sigma, T) - L_z(0, T)}{L_z(0, T)}$ where L_z corresponds to the length of the simulation box along the Cartesian z direction), and V_0 the equilibrium volume of the system. Finally, the resulting adiabatic temperature shifts were computed with the formula:

$$\Delta T(\sigma, T) = - \int_0^\sigma \frac{T}{C_\sigma(T)} d\sigma, \quad (4)$$

where $C_\sigma(T) = \left(\frac{dU}{dT} \right)_\sigma$ is the heat capacity of the crystal, which has been calculated for a dense set of stress (either hydrostatic or uniaxial) and temperature conditions.

III. RESULTS

Copper selenide exhibits two crystalline phases, a low-temperature phase (α) that is stable up to ~ 400 K and a high-temperature phase (β) that is superionic [33]. The exact

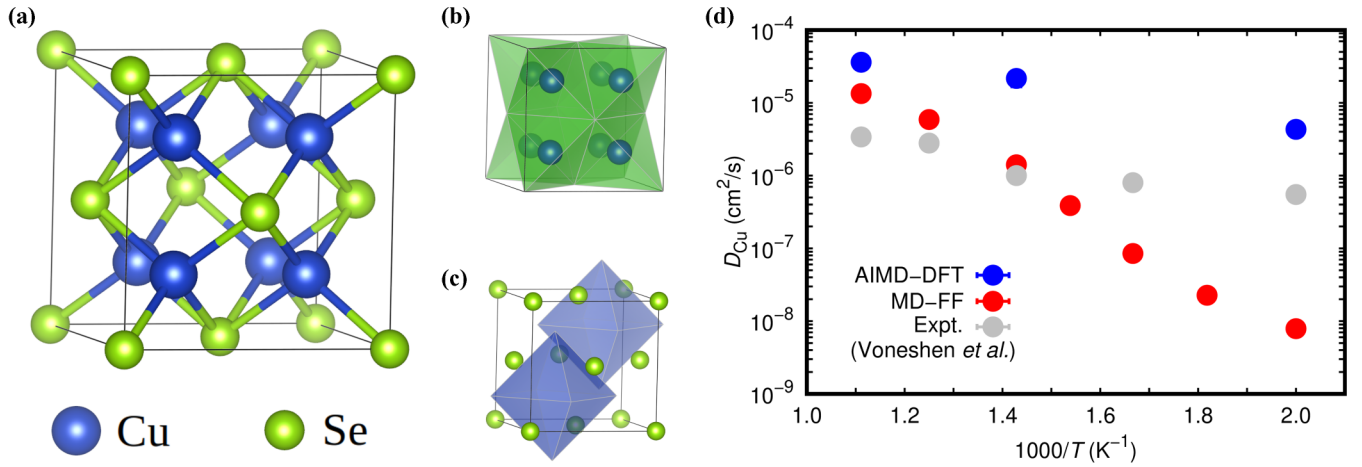


FIG. 1. General description of Cu₂Se. (a) Ball-stick representation of the high- T cubic structure known as fluorite (space group $Fm\bar{3}m$); for clarity purposes, the Cu ions are represented orderly in a simple cubic lattice. (b) Tetrahedra formed by Se ions on the vertices; the center of the tetrahedra are described by the pseudocubic Wyckoff position $8c (\frac{1}{4}, \frac{1}{4}, \frac{1}{4})$. (c) Octahedra formed by Cu ions on the vertices; the center of the octahedra are described by the pseudocubic Wyckoff position $4b (\frac{1}{2}, \frac{1}{2}, \frac{1}{2})$. (d) Ionic diffusion coefficients estimated at different temperatures from neutron spectroscopy experiments [41], first-principles calculations based on density functional theory (AIMD-DFT), and molecular dynamics simulations performed with the Morse potential reported in Ref. [29] considering null ionic charges (MD-FF).

structure of the α phase still remains under debate [34,35] although recent works have proposed that it is monoclinic with space group $P2_1/c$ [36,37]. The β phase exhibits the well-known cubic fluorite structure found in many binary fast-ion conductors (e.g., CaF₂ and UO₂) [27,38], in which the Se ions are arranged following a face-centered cubic lattice (space group $Fm\bar{3}m$) [Fig. 1(a)]. Copper ions in the β phase diffuse throughout the crystal by hopping between tetrahedral sites and off-centered octahedral interstitial positions [18,39,40] [Figs. 1(b) and 1(c)]. The critical temperature of the $\alpha \rightarrow \beta$ phase transition can be modified in practice with alloying and hydrostatic pressure as well [33].

Figure 1(d) shows the Cu diffusion coefficients, D_{Cu} , measured recently by Voneshen *et al.* at different temperatures by using neutron spectroscopy techniques [41]. D_{Cu} values of $\sim 10^{-7}$ – 10^{-6} cm² s⁻¹ have been reported within the temperature interval $500 \leq T \leq 900$ K. Our theoretical first-principles results obtained from *ab initio* molecular dynamics (AIMD) simulations systematically overestimate those experimental D_{Cu} values by roughly one order of magnitude. For instance, at $T = 500$ K (900 K) Voneshen *et al.* report 5.5×10^{-7} (3.4×10^{-6}) cm² s⁻¹ whereas we obtain 3.8×10^{-6} (4.2×10^{-5}) cm² s⁻¹. It should be mentioned, however, that in a previous experimental quasielastic neutron scattering study by Danilkin *et al.* much larger D_{Cu} values than found by Voneshen *et al.* were reported at temperatures close to the $\alpha \rightarrow \beta$ transition [18]. Specifically, a Cu diffusion coefficient of 6.1×10^{-5} cm² s⁻¹ was measured at $T = 430$ K [18], which is significantly higher than our estimations based on AIMD simulations. Hence, there seems to be a lack of quantitative agreement between the sets of experimental D_{Cu} data reported to date for β -Cu₂Se; probably additional experiments are necessary to resolve such discrepancies.

We performed molecular dynamics (MD) (N, P, T) simulations with the Morse potential proposed by Namsani *et al.* for β -Cu₂Se [29], considering both stoichiometric and off-stoichiometric systems. Unexpectedly, we found that the ionic

diffusivities estimated for all stoichiometries were practically null ($D_{Cu} < 10^{-9}$ cm² s⁻¹), even at temperatures as high as 1000 K. A possible explanation for such an overestimation in the degree of localization of copper ions in β -Cu₂Se may be that the fitting of the Morse potential reported in Ref. [29] was performed considering a perfect fluorite structure, in which the Cu atoms were arranged orderly in a simple cubic sublattice rather than occupying quasirandom positions within the crystalline Se matrix (as it occurs in the real superionic state). Moreover, the fitting of the potential parameters was performed to reproduce a number of structural and elastic properties calculated with DFT methods at zero temperature, which may not be totally relevant for the description of ionic diffusivity at high temperatures.

Incidentally, we realized that by reducing the value of the ionic charges the diffusion of the copper ions increased while the positions of the selenium atoms remained well defined. Actually, a reasonably good agreement between our MD results (considering a realistic off-stoichiometry of 2%) and the sets of experimental and AIMD D_{Cu} data was obtained for neutrally charged particles [Fig. 1(d)]. In that particular case the Cu diffusion coefficients estimated with MD at $T = 500$ K and 900 K, for instance, are 7.9×10^{-9} and 1.3×10^{-5} cm² s⁻¹, respectively. In view of these outcomes, and of the importance of accounting for ionic disorder in the simulation of superionic Cu₂Se, we decided to perform the subsequent analysis of mechanocaloric effects by adopting null ionic charges. As it is explained below, we do not expect that such a convenient (although quite arbitrary) modification of the original interatomic potential proposed by Namsani *et al.* [29] will introduce significant bias on the determination of realistic mechanocaloric effects in β -Cu₂Se.

A. Barocaloric effects

The normal (α) to superionic (β) phase transition in Cu₂Se is very promising from a barocaloric point of view since it

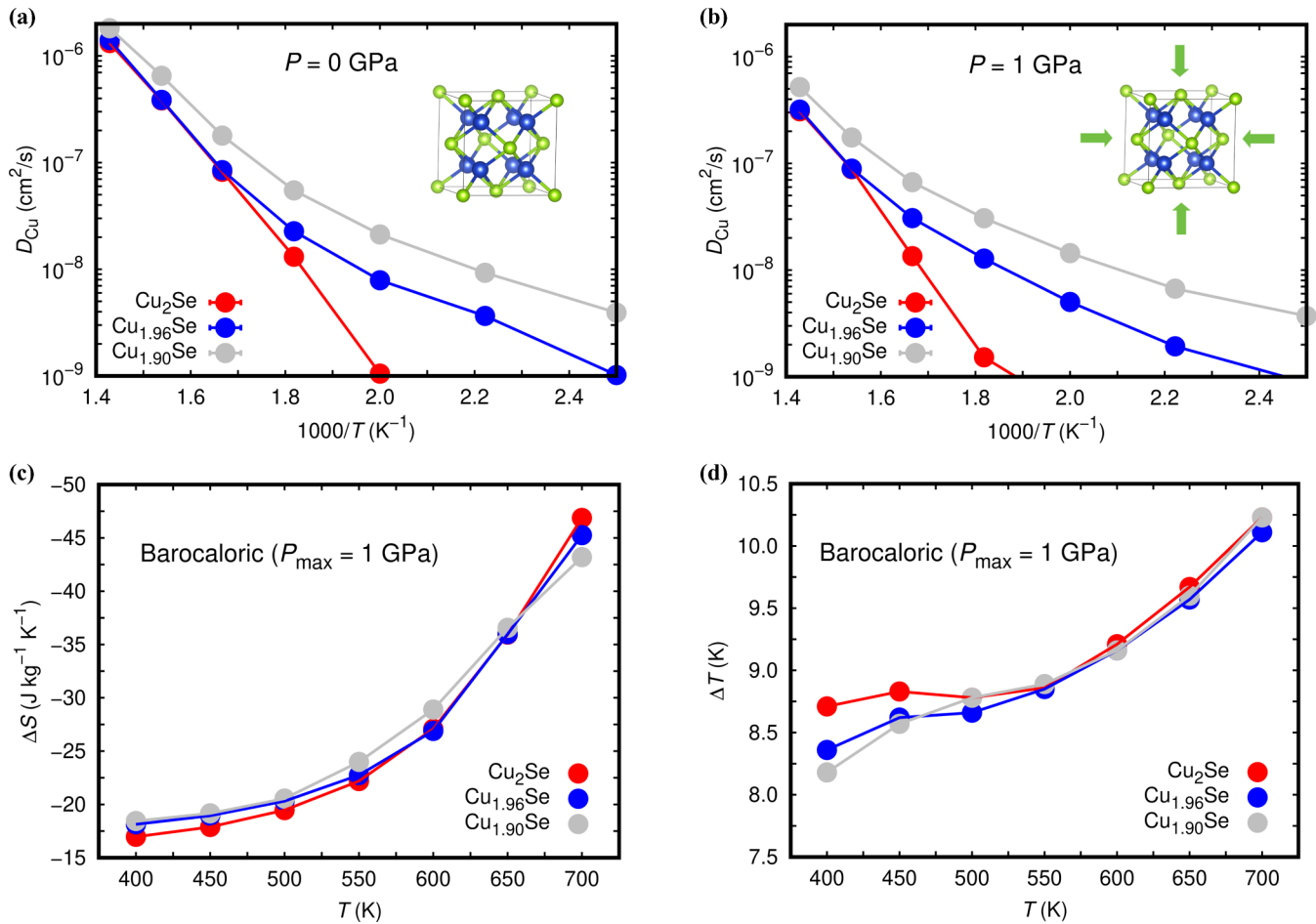


FIG. 2. Barocaloric effects in bulk $\text{Cu}_{2-\delta}\text{Se}$ at temperatures $400 \leq T \leq 700$ K. (a) Ionic diffusion coefficients calculated at zero pressure and (b) $P = 1$ GPa. (c) Isothermal entropy changes induced by a maximum hydrostatic pressure of 1 GPa. (d) Adiabatic temperature changes induced by a maximum hydrostatic pressure of 1 GPa.

involves a large change of entropy (that is, a latent heat of $|\Delta S| = 78.4 \text{ J kg}^{-1} \text{ K}^{-1}$ [42]) and it is sensitive to hydrostatic pressure P . In particular, the critical $\alpha \rightarrow \beta$ transition temperature decreases under compression according to the numerical relationship $T_{\alpha \rightarrow \beta} = 408 - 6.24P - 1.20P^2$ (where temperature is in units of K and pressure of GPa) [33]. A rough estimation of the potential barocaloric effects associated to such a first-order transition based on the experimentally reported values of the heat capacity ($C_p \approx 400 \text{ J kg}^{-1} \text{ K}^{-1}$ [16]) and latent heat, that is, $|\Delta T| = \frac{T}{C_p} |\Delta S|$ [2], leads to a colossal adiabatic temperature change of ~ 80 K. This value is much larger than the $|\Delta T|$ measured in the archetypal fast-ion conductor AgI using differential scanning calorimetry techniques (36 K), in which an analogous order-disorder phase transformation occurs close to room temperature [43]. Nevertheless, the exact nature of the low- T phase in Cu_2Se has not been determined yet unequivocally and consequently we cannot simulate that phase with reliability. Hence, we are not going to analyze here the barocaloric effects associated with the $\alpha \rightarrow \beta$ phase transition. Experimental investigations on such potentially colossal barocaloric effects are in fact highly desirable.

Meanwhile, large barocaloric effects have been recently predicted for the superionic conductor Li_3N near room

temperature, in which no structural phase transition occurs when applying moderate hydrostatic pressures on it [44]. In particular, large isothermal entropy changes of about $25 \text{ J kg}^{-1} \text{ K}^{-1}$ have been estimated at $T = 300$ K and $P = 1$ GPa, which result from stress-induced variations on the volume and ion-transport properties of the material. Here, we investigate the possible existence of barocaloric effects in $\beta\text{-Cu}_2\text{Se}$ at temperatures $400 \leq T \leq 700$ K caused by similar atomistic mechanisms than in Li_3N .

Figures 2(a) and 2(b) show the influence of hydrostatic pressure on the diffusion coefficient of copper ions in $\beta\text{-Cu}_2\text{Se}$, for which several representative stoichiometries have been considered [33]. In all the cases, ionic transport is significantly depleted under an isotropic compression of 1 GPa. For instance, at $T = 700$ K and zero pressure we estimate 1.3×10^{-6} and $1.8 \times 10^{-6} \text{ cm}^2 \text{ s}^{-1}$ for Cu_2Se and $\text{Cu}_{1.90}\text{Se}$, respectively, whereas at the same temperature and $P = 1$ GPa we obtain 3.1×10^{-7} and $5.2 \times 10^{-7} \text{ cm}^2 \text{ s}^{-1}$. Such large reductions in D_{Cu} suggest the presence of large entropy variations as induced by pressure; also, they indicate a potential enhancement in the overall thermodynamic stability of the material. Figure 2(c) reports the isothermal entropy changes that we have explicitly calculated in $\beta\text{-Cu}_2\text{Se}$ by using Eq. (2) and considering a maximum pressure of 1 GPa.

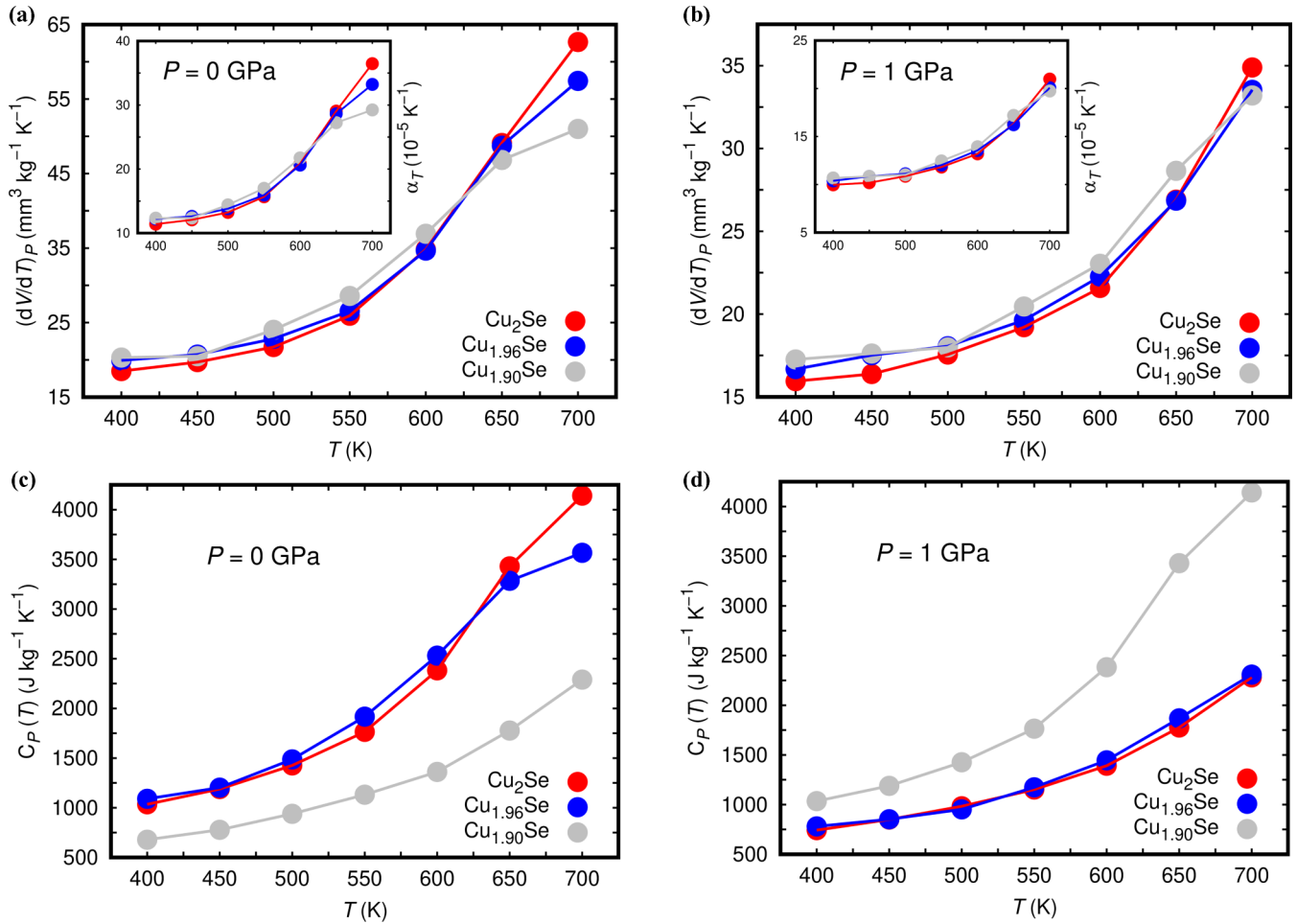


FIG. 3. Thermodynamic properties of $\text{Cu}_{2-\delta}\text{Se}$ at temperatures $400 \leq T \leq 700$ K. (a) T derivative of the volume calculated at zero pressure and (b) $P = 1$ GPa. Thermal expansion coefficients defined as $\alpha_T = \frac{1}{V}(\frac{dV}{dT})_P$ are shown in the insets. (c) Heat capacity calculated at zero pressure and (d) $P = 1$ GPa.

Such estimated entropy changes in fact turn out to be quite large. Specifically, we obtain negative values of $|\Delta S| \sim 15\text{--}45 \text{ J kg}^{-1} \text{ K}^{-1}$ throughout the selected temperature interval, in which the largest entropy variations are attained at the highest considered T .

Besides the large D_{Cu} variations caused by pressure, the intrinsically high anharmonicity of $\beta\text{-Cu}_2\text{Se}$ [18,41] appears to contribute also significantly to the estimated isothermal entropy changes (here, we somewhat arbitrarily define “anharmonicity” as any other effect different from ionic diffusivity). By carrying out additional MD simulations in which the formal cationic and anionic charges were adopted, and thus avoiding the appearance of ionic diffusion in the system (Sec. III), we found that the magnitude of the resulting barocaloric effects decreased by $\sim 60\%$ of their original values. Therefore, we conclude that the influence of thermodynamic mechanisms different from Cu diffusion on the barocaloric performance of $\beta\text{-Cu}_2\text{Se}$ is about 40%.

Figure 2(d) shows the adiabatic temperature changes estimated directly with Eq. (4) in the high- T phase of copper selenide by considering a maximum compression of 1 GPa. Large positive ΔT values of 8.50–10.25 K are obtained within the selected temperature range. The calculated adiabatic temperature shifts increase steadily with temperature for

$T \geq 500$ K and are slightly larger in the fully stoichiometric system at temperatures below that point. In Sec. IV, we will discuss and compare the magnitude of the barocaloric effects predicted for $\beta\text{-Cu}_2\text{Se}$ with those known from other materials reported in the literature.

In Fig. 3, we represent the value of the estimated T -induced volume variations and heat capacity as a function of temperature, pressure, and stoichiometry. Such properties are used directly for computing ΔS and ΔT [Eqs. (2) and (4)], hence they are very relevant from a numerical point of view. The variation of the volume with respect to temperature behaves quite regularly as a function of T and P . In particular, $(\frac{\partial V}{\partial T})_P$ displays a paraboliclike temperature dependence and it decreases under pressure [Figs. 3(a) and 3(b)]. The heat capacities computed for $\beta\text{-Cu}_2\text{Se}$ and $\text{Cu}_{1.96}\text{Se}$ exhibit similar dependences on P and T than the corresponding T derivatives of their volumes [Figs. 3(c) and 3(d)]. However, the C_P of $\beta\text{-Cu}_{1.90}\text{Se}$ presents an anomalous behavior since it increases noticeably under compression (we tentatively ascribe this tendency to some sort of effective interaction between point defects induced by P). We note that the results enclosed in Figs. 3(c) and 3(d) indicate a need for explicitly considering the P dependence of C_P in the calculation of ΔS and ΔT , since this quantity may vary quite broadly under pressure (for

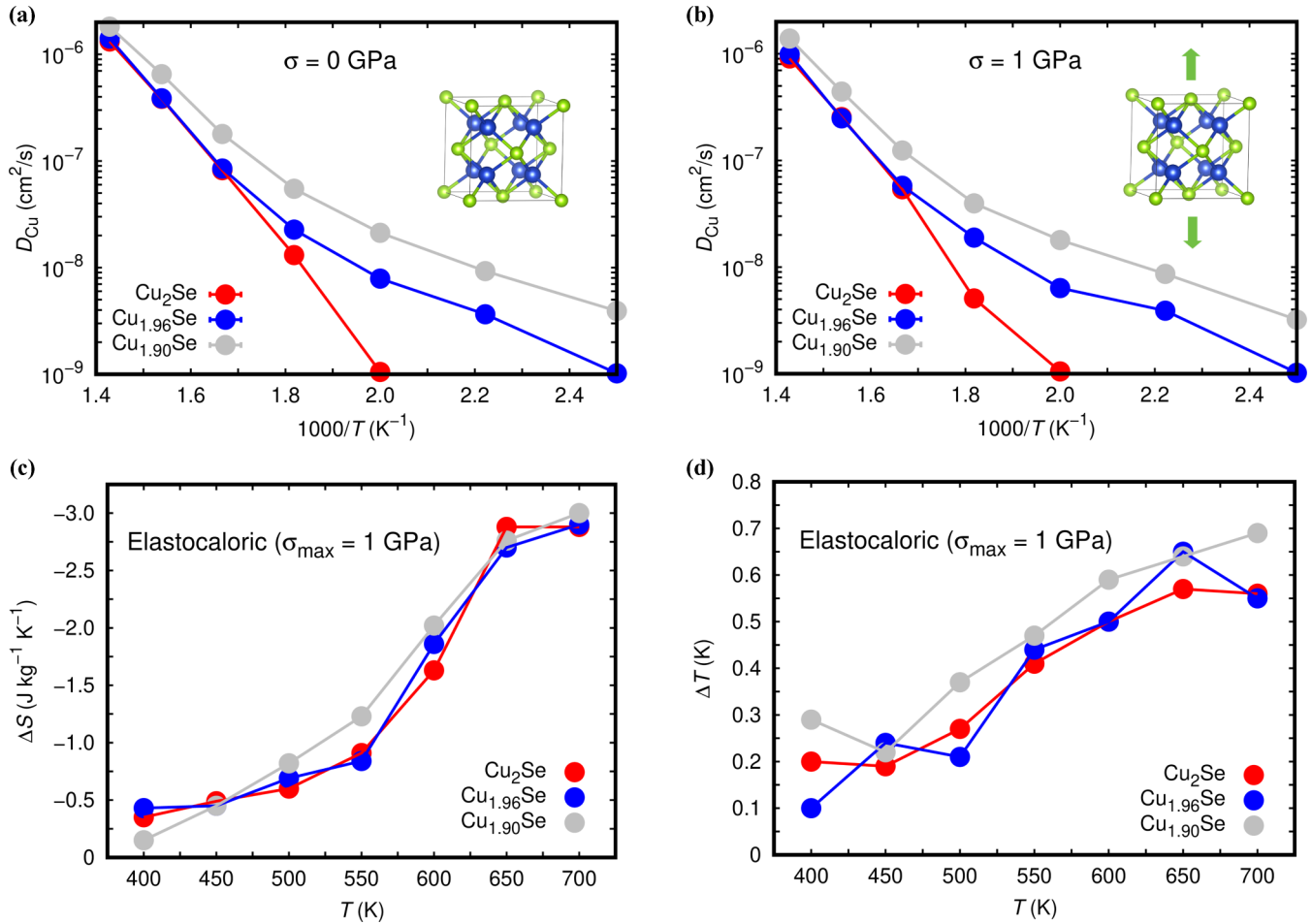


FIG. 4. Elastocaloric effects in bulk $\text{Cu}_{2-\delta}\text{Se}$ at temperatures $400 \leq T \leq 700$ K. (a) Ionic diffusion coefficients calculated at zero uniaxial tensile stress and (b) $\sigma = 1$ GPa. (c) Isothermal entropy changes induced by a maximum uniaxial tensile stress of 1 GPa. (d) Adiabatic temperature changes induced by a maximum uniaxial tensile stress of 1 GPa.

instance, at 700 K we calculate 2280 and 4141 $\text{J kg}^{-1} \text{K}^{-1}$ for the fully stoichiometric system at 1 GPa and zero pressure, respectively).

In the insets of Figs. 3(a) and 3(b), we enclose the thermal expansion coefficients, $\alpha_T = \frac{1}{V} \left(\frac{dV}{dT} \right)_P$, calculated for $\beta\text{-Cu}_2\text{Se}$ at different pressures, temperatures, and compositions. In general, we obtain much larger α_T values than measured experimentally at zero pressure [16]. For instance, at $T = 400$ K we compute $11.4 \times 10^{-5} \text{K}^{-1}$, which is about five times larger than the corresponding value determined in the experiments. A possible cause for these discrepancies may be the neglect of electrostatic cohesion in our MD simulations (Sec. III). We note that such a α_T overestimation is likely to propagate into a certain augmentation of the ΔS values reported in this work. Regarding the heat capacity, our calculations also tend to magnify considerably this quantity. For instance, at $T = 600$ K and zero pressure we compute $2383 \text{J kg}^{-1} \text{K}^{-1}$, which is about six times larger than the corresponding value determined in the experiments.

By simultaneously considering our molecular dynamics overestimation of the quantities α_T and C_P , however, we may conclude that our reported ΔT results should be pretty accurate due to a cancellation of errors between them [Eq. (4)]. Moreover, at high temperatures our ΔT results may be

regarded as a lower bound of the adiabatic temperature changes that can be achieved in practice. For instance, at $T = 700$ K the simulated α_T/C_P ratio turns out to be three times smaller than the corresponding experimental value [16]. Therefore, in spite of the inevitable shortcomings deriving from the use of classical potentials for simulating materials [45,46], we are confident that the barocaloric ΔT results reported in this work are reliable and quantitatively correct.

B. Elastocaloric effects

We have also investigated the potential of $\beta\text{-Cu}_2\text{Se}$ as a candidate elastocaloric material. In particular, we have analyzed the caloric response of the crystal under a maximum uniaxial compressive and tensile load of 1 GPa at different temperatures. Figure 4 shows the numerical ΔS and ΔT values obtained from molecular dynamics simulations in which we have considered uniaxial tensile stresses. The size of the estimated adiabatic temperature and isothermal entropy changes are about one order of magnitude smaller than calculated in the barocaloric case. For example, at $T = 400$ K we compute $\Delta S = -0.35 \text{J kg}^{-1} \text{K}^{-1}$ and $\Delta T = 0.20$ K for stoichiometric $\beta\text{-Cu}_2\text{Se}$ (to be compared with $\Delta S = -17.5 \text{J kg}^{-1} \text{K}^{-1}$ and $\Delta T = 8.7$ K obtained in the

barocaloric case). We note that the predicted elastocaloric effects present a practically negligible dependence on composition [Figs. 4(b)–4(d)]. Very similar ΔS and ΔT values have been obtained for the case of considering compressive uniaxial stresses in the simulations, which are not shown here.

Figures 4(a) and 4(b) show the influence of uniaxial tensile stress, σ , on the copper ionic diffusion coefficient of β -Cu₂Se at several temperatures. As it is appreciated therein, under a load of 1 GPa the estimated D_{Cu} 's hardly change in comparison with the values obtained at zero stress. For example, for stoichiometric Cu₂Se at $T = 700$ K and $\sigma = 0$ we estimate $1.3 \times 10^{-6} \text{ cm}^2 \text{ s}^{-1}$ whereas at the same temperature and $\sigma = 1$ GPa we obtain $1.0 \times 10^{-6} \text{ cm}^2 \text{ s}^{-1}$. Such a small σ -induced reduction in the ionic diffusivity, and therefore in the entropy of the system, explains the minuteness and sign of the elastocaloric effects predicted for β -Cu₂Se [Eq. (3)]. We note in passing that Cu₂Se and thermoelectric materials in general are brittle hence in practice cannot withstand large uniaxial stresses [47]. Consequently, it may be concluded that thermoelectric compounds presenting high ionic disorder in principle are not promising elastocaloric materials.

IV. DISCUSSION

To date, large barocaloric effects have been experimentally measured in a number of shape-memory alloys [48,49], polar compounds [50,51], organic-inorganic hybrid perovskites [52], molecular crystals [53–55], and the archetypal fast-ion conductor AgI [43]. In Table I, we list several representative barocaloric compounds along with some of their basic cooling features measured at or near room temperature (made the exception of Li₃N [44], for which barocaloric experiments have not been performed yet). The thermoelectric fast-ion conductor β -Cu₂Se in fact turns out to be competitive with those archetypal materials in terms of barocaloric performance.

The isothermal entropy change induced by a hydrostatic pressure of 1 GPa in β -Cu₂Se at $T = 400$ K is relatively small as compared to those measured, for instance, in the shape-memory alloy Ni₅₁Mn₃₃In₁₆, the ferroelectric salt

(NH₄)₂SO₄, the molecular crystal (CH₃)₂C(CH₂OH)₂, and the fast-ion conductor AgI (Table I). On the other hand, the $|\Delta S|$ estimated for copper selenide is larger than or similar in magnitude to those found in the shape-memory alloy Fe₄₉Rh₅₁ and the archetypal ferroelectric BaTiO₃. In terms of adiabatic temperature shift, which arguably is the most important quality of caloric materials, β -Cu₂Se is better positioned. The calculated $|\Delta T|$ of 8.7 K is larger than most values reported in Table I, made the remarkable exceptions of the molecular crystal (CH₃)₂C(CH₂OH)₂ and the fast-ion conductor AgI. It should be mentioned, however, that the experimental barocaloric effects that we review here have been obtained for hydrostatic pressures significantly smaller than 1 GPa. For this reason, the predicted barocaloric strength of β -Cu₂Se, which is defined as the ratio $|\Delta T|/P$, is not particularly exceptional ($\sim 10 \text{ K GPa}^{-1}$).

It is interesting to compare the barocaloric performance of β -Cu₂Se with that of Li₃N since both compounds are superionic and the corresponding $|\Delta S|$ and $|\Delta T|$ values have been obtained with similar computational methods [44]. The isothermal entropy change estimated in Li₃N is practically two times larger than the value found in β -Cu₂Se under same T and P conditions. The main reason for such a difference is that the ionic diffusivity in Li₃N is much larger than that in β -Cu₂Se (10^{-3} versus $10^{-9} \text{ cm}^2 \text{ s}^{-1}$, respectively), and thus the changes in ionic mobility caused by compression also result larger in Li₃N. Nevertheless, the adiabatic temperature change predicted for β -Cu₂Se is $\sim 60\%$ larger than for Li₃N. This outcome results from the substantially smaller heat capacity that is calculated for the thermoelectric crystal (namely, the C_p of Li₃N is about an order of magnitude larger than that of β -Cu₂Se [44]). In view of these findings, we propose that an effective design strategy for enhancing likely mechanocaloric effects in fast-ion conductors may consist in optimizing the corresponding heat capacities (that is, making them as small as possible by means of composition, for instance).

It is worth reminding that the “giant” barocaloric effects (i.e., $|\Delta T| > 10 \text{ K}$) measured in the also fast-ion conductor AgI (Table I) were obtained for its normal to superionic phase

TABLE I. Materials presenting large ($|\Delta T| > 1 \text{ K}$) or giant ($|\Delta T| > 10 \text{ K}$) barocaloric effects at or near room temperature. T represents working temperature, P applied pressure, $|\Delta S|$ isothermal entropy change, $|\Delta T|$ adiabatic temperature change, $|\Delta T|/P$ barocaloric strength, “SMA” shape-memory alloy, “FE” ferroelectric, “OIH” organic-inorganic hybrid perovskite, “MC” molecular crystal, “FIC” fast-ion conductor, and “TE” thermoelectric.

	T (K)	P (GPa)	$ \Delta S $ (JK ⁻¹ Kg ⁻¹)	$ \Delta T $ (K)	$ \Delta T /P$ (K GPa ⁻¹)	Materials type	Reference
Ni ₅₁ Mn ₃₃ In ₁₆	330	0.25	41.0	4.0	16.0	SMA	[48]
Fe ₄₉ Rh ₅₁	310	0.11	12.5	8.1	73.6	SMA	[49]
BaTiO ₃	400	0.10	2.4	1.0	10.0	FE	[50]
(NH ₄) ₂ SO ₄	220	0.10	130.0	8.0	80.0	FE	[51]
[TPrA][Mn(dca) ₃]	330	0.01	30.5	4.1	410.0	OIH	[52]
[FeL ₂][BF ₄] ₂	262	0.03	80.0	3.0	100.0	MC	[53]
(CH ₃) ₂ C(CH ₂ OH) ₂	320	0.52	510.0	45.0	86.5	MC	[54,55]
AgI	400	0.25	62.0	36.0	144.0	FIC	[43]
Li ₃ N	400	1.00	33.5	5.4	5.4	FIC	[44]
Cu ₂ Se	400	1.00	17.5	8.7	8.7	TE/FIC	This work

transition, which is of first-order type and has associated a large latent heat [43]. Copper selenide also presents a $\alpha \rightarrow \beta$ phase transition near room temperature [33] but for the reasons explained above (e.g., indetermination of the corresponding low- T phase) we have restricted our analysis here to mechanocaloric effects occurring in the high- T phase. Such mechanocaloric effects turn out to be large and are mostly due to continuous changes in the ionic diffusivity caused by pressure. Actually, the kind of second-order-like changes disclosed here for β -Cu₂Se present great prospects in the context of refrigeration-cycle reversibility owing to the likely absence of mechanical hysteresis effects deriving from the nucleation of order-parameter domains [44]. Nevertheless, our rough estimation of $|\Delta T| \sim 80$ K for the normal to superionic phase transition in Cu₂Se (Sec. III A), and the previous success achieved in AgI for the same type of transformation (Table I) [43], should motivate also experimental searches of giant barocaloric effects in thermoelectric fast-ion conductor materials near room temperature.

V. CONCLUSIONS

Copper selenide and other similar silver- and sulfide-based compounds (e.g., Cu₂S, Cu₂Te, Ag₂Se, Ag₂S, Ag₂Te, and Cu_{2-x}Ag_xX (X = S, Se and Te) alloys) are thermoelectric fast-ion conductor materials for which huge thermoelectric figures of merit have been reported. However, owing to their ionic transport properties these materials are prone to suffer severe structural degradation when subjected to intense electric fields. In this computational work, we have shown that by applying moderate hydrostatic pressures of ~ 1 GPa

it is possible to reduce significantly the ionic diffusivity of Cu₂Se, thus improving its thermodynamic stability, and to induce large barocaloric effects near room temperature. It is very likely that similar P -induced phenomena will occur also in analogous thermoelectric superionic materials.

The caloric response of Cu₂Se is mostly originated by substantial changes on its ionic conductivity caused by compression. Such large barocaloric effects, namely, $|\Delta S| \sim 17.5 \text{ J kg}^{-1} \text{ K}^{-1}$ and $|\Delta T| = 8.7 \text{ K}$ at $T = 400 \text{ K}$, are very promising for engineering novel solid-state cooling applications that do not require the application of electric fields. In this context, thermoelectric superionic materials are free of the degradation and energy-efficiency problems affecting solid-state refrigeration based on the Peltier effect. Moreover, we foresee the existence of colossal barocaloric effects ($|\Delta T| \gg 10 \text{ K}$) associated with the normal to superionic phase transition that occurs in Cu₂Se near room temperature (not simulated explicitly in this study). Hence, our theoretical findings on Cu₂Se should stimulate new energy-conversion experiments in thermoelectric fast-ion conductors that potentially can lead to robust and highly efficient solid-state cooling applications.

ACKNOWLEDGMENTS

Computational resources and technical assistance were provided by the Australian Government and the Government of Western Australia through the National Computational Infrastructure (NCI) and Magnus under the National Computational Merit Allocation Scheme and The Pawsey Supercomputing Centre.

-
- [1] C. Cazorla, Refrigeration based on plastic crystals, *Nature (London)* **567**, 470 (2019).
 - [2] X. Moya, S. Kar-Narayan, and N. D. Mathur, Caloric materials near ferroic phase transitions, *Nat. Mater.* **13**, 439 (2014).
 - [3] D. Zhao and G. Tan, A review of thermoelectric cooling: Materials, modeling and applications, *Appl. Therm. Eng.* **66**, 15 (2014).
 - [4] C. Cazorla and J. Íñiguez, Giant direct and inverse electrocaloric effects in multiferroic thin films, *Phys. Rev. B* **98**, 174105 (2018).
 - [5] T. Krenke, E. Duman, E. Acet, E. F. Wassermann, X. Moya, Ll. Mañosa, and A. Planes, Inverse magnetocaloric effect in ferromagnetic Ni-Mn-Sn alloys, *Nat. Mater.* **4**, 450 (2005).
 - [6] E. Defay, S. Crossley, S. Kar-Narayan, X. Moya, and N. D. Mathur, The electrocaloric efficiency of ceramic and polymer films, *Adv. Mater.* **25**, 3337 (2013).
 - [7] Ll. Mañosa and A. Planes, Materials with giant mechanocaloric effects: Cooling by strength, *Adv. Mater.* **29**, 1603607 (2017).
 - [8] A. K. Sagotra, D. Errandonea, and C. Cazorla, Mechanocaloric effects in superionic thin films from atomistic simulations, *Nat. Commun.* **8**, 963 (2017).
 - [9] J. Tusek, K. Engelbrecht, R. Millán-Solsona, Ll. Mañosa, E. Vives, L. P. Mikkelsen, and N. Pryds, The elastocaloric effect: A way to cool efficiently, *Adv. Energy Mater.* **5**, 1500361 (2015).
 - [10] C. Cazorla, Novel mechanocaloric materials for solid-state cooling applications, *Appl. Phys. Rev.* **6**, 041316 (2019).
 - [11] C. B. Zimm, A. Jastrab, A. Sternberg, V. Pecharsky, K. Gschneidner, M. Osborne, and I. Anderson, Description and performance of a near-room temperature magnetic refrigerator, *Adv. Cryog. Eng.* **43**, 1759 (1998).
 - [12] G. J. Snyder, J.-P. Fleurial, and T. Caillat, Supercooling of peltier cooler using a current pulse, *J. Appl. Phys.* **92**, 1564 (2002).
 - [13] A. Zevalkink, D. M. Smiadak, J. L. Blackburn, A. J. Ferguson, M. L. Chabinyk, O. Delaire, J. Wang, K. Kovnir, J. Martin, L. T. Schelhas *et al.*, A practical field guide to thermoelectrics: Fundamentals, synthesis, and characterization, *Appl. Phys. Rev.* **5**, 021303 (2018).
 - [14] E. Haque, C. Cazorla, and M. A. Hossain, First-principles prediction of large thermoelectric efficiency in superionic Li₂SnX₃ (X = S, Se), *Phys. Chem. Chem. Phys.* **22**, 878 (2020).
 - [15] S. A. Tassou, J. S. Lewis, Y. T. Ge, A. Hadaway, and I. Chaer, A review of emerging technologies for food refrigeration applications, *Appl. Therm. Eng.* **30**, 263 (2010).
 - [16] H. Liu, X. Shi, F. Xu, L. Zhang, W. Zhang, L. Chen, Q. Li, C. Uher, T. Day, and G. J. Snyder, Copper ion liquid-like thermoelectrics, *Nat. Mater.* **11**, 422 (2012).
 - [17] S. Hull, Superionics: Crystal structures and conduction processes, *Rep. Prog. Phys.* **67**, 1233 (2004).
 - [18] S. A. Danilkin, M. Avdeev, M. Sale, and T. Sakuma, Neutron scattering study of ionic diffusion in Cu-Se superionic compounds, *Solid State Ion.* **225**, 190 (2012).

- [19] H. Kim, S. Ballikaya, H. Chi, J.-P. Ahn, K. Ahn, C. Uher, and M. Kaviani, Ultralow thermal conductivity of β -Cu₂Se by atomic fluidity and structure distortion, *Acta Mater.* **86**, 247 (2015).
- [20] S. Ballikaya, H. Chi, J. R. Salvador, and C. Uher, Thermoelectric properties of Ag-doped Cu₂Se and Cu₂Te, *J. Mater. Chem. A* **1**, 12478 (2013).
- [21] D. R. Brown, T. Day, K. A. Borup, S. Christensen, B. B. Iversen, and G. F. Snyder, Phase transition enhanced thermoelectric figure-of-merit in copper chalcogenides, *APL Mater.* **1**, 052107 (2013).
- [22] C. Han, Q. Sun, Z. Li, and S. X. Dou, Thermoelectric enhancement of different kinds of metal chalcogenides, *Adv. Ener. Mater.* **6**, 1600498 (2016).
- [23] T. P. Bailey and C. Uher, Potential for superionic conductors in thermoelectric applications, *Curr. Opin. Green Sust. Chem.* **4**, 58 (2017).
- [24] G. Dennler, R. Chmielowski, S. Jacob, F. Capet, P. Roussel, S. Zastrow, K. Nielsch, I. Opahle, and G. K. H. Madsen, Are binary copper sulfides/selenides really new and promising thermoelectric materials? *Adv. Ener. Mater.* **4**, 1301581 (2014).
- [25] C. Cazorla and D. Errandonea, Comment on high-pressure phases of group-ii difluorides: Polymorphism and superionicity, *Phys. Rev. B* **98**, 186101 (2018).
- [26] A. K. Sagotra, D. Chu, and C. Cazorla, Influence of lattice dynamics on lithium-ion conductivity: A first-principles study, *Phys. Rev. Mater.* **3**, 035405 (2019).
- [27] C. Cazorla and D. Errandonea, Superionicity and Polymorphism in Calcium Fluoride at High Pressure, *Phys. Rev. Lett.* **113**, 235902 (2014).
- [28] S. J. Plimpton, Fast parallel algorithms for short-range molecular dynamics, *J. Comp. Phys.* **117**, 1 (1995); <http://lammps.sandia.gov>.
- [29] S. Namsani, B. Gahtori, S. Auluck, and J. K. Singh, An interaction potential to study the thermal structure evolution of a thermoelectric material: β -Cu₂Se, *J. Comput. Chem.* **38**, 2161 (2017).
- [30] G. Kresse and J. Furthmüller, Efficient iterative schemes for ab initio total-energy calculations using a plane-wave basis set, *Phys. Rev. B* **54**, 11169 (1996).
- [31] J. P. Perdew, K. Burke, and M. Ernzerhof, Generalized Gradient Approximation Made Simple, *Phys. Rev. Lett.* **77**, 3865 (1996).
- [32] P. E. Blöchl, Projector augmented-wave method, *Phys. Rev. B* **50**, 17953 (1994).
- [33] J. B. Clark and E. Rapoport, Effect of pressure on solid-solid transitions in some silver and cuprous chalcogenides, *J. Phys. Chem. Solids* **31**, 247 (1970).
- [34] H. Liu *et al.*, Ultrahigh thermoelectric performance by electron and phonon critical scattering in Cu₂Se_{1-x}I_x, *Adv. Mater.* **25**, 6607 (2013).
- [35] L. Gulay, M. Daszkiewicz, O. Strok, and A. Pietraszko, Crystal structure of Cu₂Se, *Chem. Met. Alloys* **4**, 200 (2011).
- [36] M. C. Nguyen, J.-H. Choi, C.-Z. Wang, Z. Zhang, and H.-M. Ho, New Layered Structures of Cuprous Chalcogenides as Thin Film Solar Cell Materials: Cu₂Te and Cu₂Se, *Phys. Rev. Lett.* **111**, 165502 (2013).
- [37] H. Chi, H. Kim, J. C. Thomas, G. Shi, K. Sun, M. Abeykoon, E. S. Bozin, X. Shi, Q. Li, X. Shi *et al.*, Low-temperature structural and transport anomalies in Cu₂Se, *Phys. Rev. B* **89**, 195209 (2014).
- [38] C. Cazorla, D. Errandonea, Giant mechanocaloric effects in fluorite-structured superionic materials, *Nano Lett.* **16**, 3124 (2016).
- [39] C. Cazorla, A. K. Sagotra, M. King, and D. Errandonea, High-pressure phase diagram and superionicity of alkaline-earth metal difluorides, *J. Phys. Chem. C* **122**, 1267 (2018).
- [40] A. K. Sagotra and C. Cazorla, Stress-mediated enhancement of ionic conductivity in fast-ion conductors, *ACS Appl. Mater. Interfaces* **9**, 38773 (2017).
- [41] D. J. Voneshen, H. C. Walker, K. Refson, and J. P. Goff, Hopping Time Scales and the Phonon-Liquid Electron-Crystal Picture in Thermoelectric Copper Selenide, *Phys. Rev. Lett.* **118**, 145901 (2017).
- [42] R. M. Murray and R. D. Heyding, The copper-selenium system at temperatures to 850 K and pressures to 50 kbar, *Can. J. Chem.* **53**, 878 (1975).
- [43] A. Aznar, P. Lloveras, M. Romanini, M. Barrio, J. Ll. Tamarit, C. Cazorla, D. Errandonea, N. D. Mathur, A. Planes, X. Moya, and Ll. Mañosa, Giant barocaloric effects over a wide temperature range in superionic conductor AgI, *Nat. Commun.* **8**, 1851 (2017).
- [44] A. K. Sagotra, C. Dewei, and C. Cazorla, Room-temperature mechanocaloric effects in lithium-based superionic materials, *Nat. Commun.* **9**, 3337 (2018).
- [45] C. Cazorla and J. Boronat, Simulation and understanding of atomic and molecular quantum crystals, *Rev. Mod. Phys.* **89**, 035003 (2017).
- [46] Q. Lai, Y. Sun, T. Wang, P. Modi, C. Cazorla, U. B. Demirci, J. R. A. Fernandez, F. Leardini, and K.-F. Aguey-Zinsou, How to design hydrogen storage materials? Fundamentals, synthesis, and storage tanks, *Adv. Sustainable Syst.* **3**, 1900043 (2019).
- [47] K. Tyagi, B. Gahtori, S. Bathula, M. Jayasimhadri, S. Sharma, N. K. Singh, D. Haranath, A. K. Srivastava, and A. Dhar, Crystal structure and mechanical properties of spark plasma sintered Cu₂Se: An efficient photovoltaic and thermoelectric material, *Solid State Commun.* **207**, 21 (2015).
- [48] E. Stern-Taulats, A. Planes, P. Lloveras, M. Barrio, J.-Ll. Tamarit, S. Pramanick, S. Majumdar, S. Yüce, B. Emre, C. Frontera, and Ll. Mañosa, Tailoring barocaloric and magnetocaloric properties in low-hysteresis magnetic shape memory alloys, *Acta Mater.* **96**, 324 (2015).
- [49] E. Stern-Taulats, A. Gracia-Condal, A. Planes, P. Lloveras, M. Barrio, J.-Ll. Tamarit, S. Pramanick, S. Majumdar, and Ll. Mañosa, Reversible adiabatic temperature changes at the magnetocaloric and barocaloric effects in Fe₄₉Rh₅₁, *Appl. Phys. Lett.* **107**, 152409 (2015).
- [50] Stern-Taulats, P. Lloveras, M. Barrio, E. Defay, M. Egilmez, A. Planes, J.-Ll. Tamarit, Ll. Mañosa, N. D. Mathur, and X. Moya, Inverse barocaloric effects in ferroelectric BaTiO₃ ceramics, *APL Mater.* **4**, 091102 (2016).
- [51] P. Lloveras, E. Stern-Taulats, M. Barrio, J.-Ll. Tamarit, S. Crossley, W. Li, V. Pomjakushin, A. Planes, Ll. Mañosa, N. D. Mathur, and X. Moya, Giant barocaloric effects at low temperature in ferroelectric ammonium sulphate, *Nat. Commun.* **6**, 8801 (2015).
- [52] J. M. Bermúdez-García, M. Sánchez-Andújar, S. Castro-García, J. López-Beceiro, R. Artiaga, and M. A. Señarís-Rodríguez, Giant barocaloric effect in the ferroic organic-inorganic hybrid

- [TPrA][Mn(dca)₃] perovskite under easily accessible pressures, *Nat. Commun.* **8**, 15715 (2017).
- [53] S. P. Vallone, A. N. Tantillo, A. M. dos Santos, J. J. Molaison, R. Kulmaczewski, A. Chapoy, P. Ahmadi, M. A. Halcrow, and K. G. Sandeman, Giant Barocaloric effect at the spin crossover transition of a molecular crystal, *Adv. Mater.* **31**, 1807334 (2019).
- [54] B. Li *et al.*, Colossal barocaloric effects in plastic crystals, *Nature (London)* **567**, 506 (2019).
- [55] P. Lloveras, A. Aznar, M. Barrio, Ph. Negrier, C. Popescu, A. Planes, Ll. Mañosa, E. Stern-Taulats, A. Avramenko, N. D. Mathur, X. Moya, and J.-Ll. Tamari, Colossal barocaloric effects near room temperature in plastic crystals of neopentylglycol, *Nat. Commun.* **10**, 1803 (2019).